Math. Model. Nat. Phenom.
Vol. 10, No. 4, 2015, pp. 61–75
DOI: 10.1051/mmnp/201510403

Hysteresis of Contact Angle of Sessile Droplets

I. Kuchin, V. Starov *

Department of Chemical Engineering, Loughborough University, LE11 3TU, UK.

Abstract. A theory of contact angle hysteresis on smooth, homogeneous solid substrates is developed in terms of shape of disjoining/conjoining pressure isotherm and quasi-equilibrium phenomena. It is shown that all contact angles, θ, in the range $\theta_r<\theta<\theta_a$, which are different from the unique equilibrium value θ_e, correspond to the state of slow "microscopic" advancing or receding motion of the liquid if $\theta_e<\theta<\theta_a$ or $\theta_r<\theta<\theta_e$, respectively. This "microscopic" motion almost abruptly becomes fast "macroscopic" advancing or receding motion after the contact angle reaches the critical values θ_a or θ_r, correspondingly. The values of the static receding, θ_r, and static advancing,θ_a, contact angles in cylindrical capillaries were calculated earlier, based on the shape of disjoining/conjoining pressure isotherm. It is shown that both advancing contact and receding contact angles of a droplet on a solid substrate depends on the drop volume and are not a unique characteristic of the liquid-solid system. The suggested mechanism of the contact angle hysteresis of droplets has direct experimental confirmation.

Keywords and phrases: contact angle hysteresis, surface forces

Mathematics Subject Classification: 76B45, 76D45, 76D05, 76R50, 82D15

1. Introduction

Why do droplets of different liquids deposited on the identical solid substrate behave so differently? Why identical droplets, for example, aqueous droplets, deposited on different substrates behave also differently?

As known, a mercury droplet does not spread on a glass substrate. It rather forms a spherical cap with the contact angle bigger than $\pi/2$. An aqueous droplet deposited on the identical glass substrate spreads only partially down to some contact angle,θ, which is in between 0 and $\pi/2$. However, an oil droplet (hexane or decane) deposited on the same glass substrate spreads out completely, and the contact angle decreases with time down to the zero value. Needless to say, that these three cases which are referred to as: non-wetting, partial wetting and complete wetting, respectively, are determined by the nature of both the liquid and the solid substrate and their interactions. Manifestation of this interaction is disjoining/conjoining pressure.

It is usually believed that the generally known phenomenon of static hysteresis of the contact angle is determined by the surface roughness and/or heterogeneity. No doubt that a roughness and/or a chemical heterogeneity of the solid substrate contribute substantially to the contact angle hysteresis. In this case it is assumed that at each point of the surface the equilibrium value of the contact angle is established, depending only on the local properties of the substrate. As a result, a whole series of local thermodynamic

*Corresponding author. E-mail: V.M.Starov@lboro.ac.uk

equilibrium states can be realized, corresponding to a certain interval of values of the contact angle. The maximum possible value corresponds to the value of the static advancing contact angle, θ_a, and the minimum possible value corresponds to the static receding contact angle, θ_r. Hence, the dependency of the contact angle on the velocity of motion of a meniscus or a drop can be qualitatively described by the dependency presented in Fig.1 (bold lines 1).

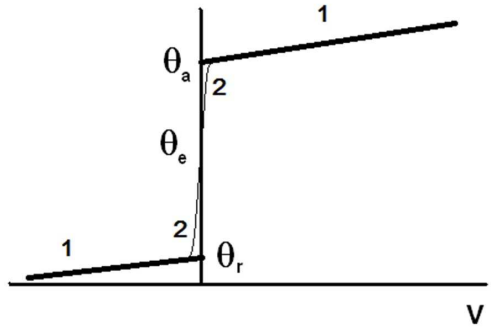

FIGURE 1. Bold lines 1: Idealised dependency of the contact angle on the advancing (v>0) or the receding (v<0) velocity of a droplet/meniscus. All contact angles, θ, between static advancing contact angle, θ_a, and static receding contact angle, θ_r , are considered as equilibrium contact angles. Curve 2: a real dependency of the contact angle on the advancing or receding velocities. At any deviation from the equilibrium contact angle, θ_e, the liquid drop/meniscus is in the state of a slow "microscopic motion", which almost abruptly transforms into "a macroscopic motion". Static advancing and receding contact angles, θ_a and θ_r, are extrapolations to zero velocity.

However, roughness and/or heterogeneity of the surface are apparently not the sole reasons for contact angle hysteresis. Over the last years there have been an increasing number of publications which confirmed the presence of contact angle hysteresis even on smooth, homogeneous surfaces [6-11]. However, the most convincing evidence for the presence of the above mentioned phenomenon is its presence on free liquid films [12-16]: in this case there is a hysteresis of a meniscus which free films are in contact with. In the latter case, the surfaces of free liquid films are not rough at all and are chemically homogeneous also. Hence, in the case of contact angle hysteresis on free liquid films it is impossible to explain the hysteresis phenomenon by the presence of roughness and/or heterogeneity.

Below we describe a mechanism of contact angle hysteresis based on the consideration of surface forces, which act in the vicinity of the three-phase contact line. This type of contact angle hysteresis is present even on a smooth, homogeneous substrate. Consideration of this kind of contact angle hysteresis on rough and/or non-homogeneous surfaces from this point of view is to be undertaken.

Evidently only a single unique value of equilibrium contact angle, θ_e, is possible on a smooth, homogeneous surface. Hence, the hysteresis contact angles $\theta_a \neq \theta_e$, $\theta_r \neq \theta_e$ and all contact angles in between, which are observed experimentally on such surfaces, correspond only to non-equilibrium states of the system. Hence, the picture presented by bold lines in Fig. 1 should be replaced by a new more realistic picture presented in the same picture by curve 2.

Thus, below the discussion of the hysteresis phenomenon is based on the analysis of non-equilibrium states of the system: menisci and/or droplets on smooth homogeneous solid substrate.

2. The disjoining/conjoining pressure components

Earlier a theory of contact angle hysteresis of menisci in thin capillaries has been developed [1,2] based on a s-shape of disjoining/conjoining pressure isotherm. What are the physical phenomena which result in formation of a disjoining/conjoining pressure [1,2]? It is obvious that properties of liquid in a vicinity of liquid-air and solid-liquid interfaces differ from the corresponding properties in the bulk. We refer to these layers as boundary layers (nothing to do with hydrodynamic boundary layers). In a vicinity of an apparent three phase contact line these boundary layer overlap (regions 3 and 4 in Fig. 2). This overlapping of boundary layers is the reason why disjoining/conjoining pressure to appear.

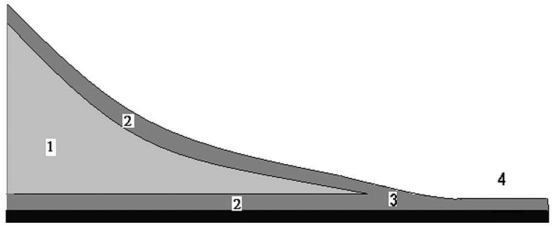

FIGURE 2. Equilibrium drop and the liquid profile in vicinity of the apparent three-phase contact line. 1 - bulk liquid, where boundary layers do not overlap, 2 – boundary layer in the vicinity of liquid-air and liquid – solid interfaces; 3 – a region, where boundary layers overlap, 4 – flat thin equilibrium film. The latter two are the regions where disjoining/conjoining pressure acts.

Contact angle hysteresis on smooth homogeneous substrates appears in the case of partial wetting, when disjoining/conjoining isotherm has a special s-shape. Components contributing to the formation of disjoining/conjoining pressure are discussed in [3-5]. These components are electrostatic component, which is caused by surface charges formation and overlapping of electrical double layers:

$$\Pi_E = RTc_0\left(\exp(\psi)+\exp(-\psi)\right) - 2RTc_0 - \frac{(RT)^2\varepsilon\varepsilon_0}{2F^2}\left(\frac{\partial\psi}{\partial y}\right)^2, \tag{2.1}$$

where R,T, F, ϵ, ϵ_0 are universal gas constant, temperature in ^{o}K, dielectric constant of water and dielectric constant of vacuum, respectively; c_0 is electrolyte concentration; y and ψ are the co-ordinate normal to the liquid-air interface and dimensionless electric potential in F/RT units;
Structural component, which is caused by water molecule dipoles orientation in a vicinity of interfaces and overlapping of these structured layers [3,4]:

$$\Pi_S = K_1\exp\left(-h/\lambda_1\right) + K_2\exp\left(-h/\lambda_2\right), \tag{2.2}$$

where K_1, K_2 and λ_1, λ_2 are parameters related to the magnitude and the characteristic length of the structural forces. The indexes 1 and 2 correspond to the short-range and long-range structural interactions, respectively. All the latter four constants should be extracted from experimental data;
Molecular or Wan-der-Waals component [3,4]:

$$\Pi_M(h) = \frac{A}{6\pi h^3}, \tag{2.3}$$

where $A = -A_H$, A_H is the Hamaker constant. The importance of the last component is usually grossly exaggerated in the literature. Note, $\Pi_M(h) \to \infty$ at $h \to 0$, however, disjoining pressure is a macroscopic value, that is valid only at h>> molecular dimension. Under the latter condition other components of the disjoining pressure become equally or more important in the case of aqueous solutions.

The resulting disjoining/conjoining isotherm has a characteristic s-shape [1,2]

$$\Pi(h) = \Pi_M(h) + \Pi_E(h) + \Pi_S(h). \tag{2.4}$$

The structural forces can arise due to the changes in the orientation structure of polar liquid near the surface [1,3-4]. Particularly, the force between the hydrophobic surfaces in water can be described by the short-range term or by a combination of the short- and long-range terms as given in Eq.(2.2). These two terms of structural interaction are denoted in Eq.(2.2) by the indexes 1 and 2, respectively. An example of the structural components calculation using Eq.(2.2) is shown in Fig.3.

The parameters K_1, K_2 correspond to the maximum values of the structural forces at zero separations h. The length parameters λ_1, λ_2 can be considered as the distances corresponding approximately to a half-decay of the structural forces. The short-range forces are usually characterized by values of λ_1 equal to a few nanometers; the long-range interaction is observed at distances up to 100 nm with values λ_2 = 13-62 nm [4]. For example, in the case of hydrophobic attraction in water between mica surfaces of crossed cylinders hydrophobized by the adsorption layers of fluorocarbon surfactant: λ_1= 2-3 nm, $\lambda_2 \approx$ 16 nm [4].

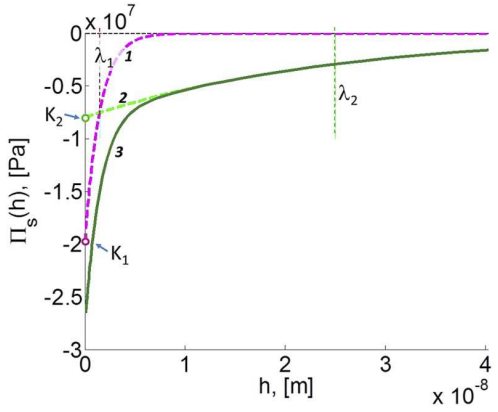

FIGURE 3. The components of the structural interaction. 1- short-range interaction, $K_1\exp(-h/\lambda_1)$; 2- long-range interaction, $K_2\exp(-h/\lambda_2)$; 3 - the total structural interaction, $K_1\exp(-h/\lambda_1) + K_2\exp(-h/\lambda_2)$. K_1 = -2×10^7 Pa; λ_1 = 1.5×10^{-9} m;K_2 = -8×10^6 Pa; λ_2 = 25×10^{-9} m.

In the case of the short-range structural interaction only, the disjoining/conjoining pressure isotherms obtained as a sum of the electrostatic, van der Waals and structural interactions can include a single primary minimum. However, the long-range structural forces can cause an additional secondary minimum in the isotherm (Fig.4). A depth and position of these both minima are determined by parameters of the structural interactions in combination with the parameters of the electrostatic and van der Waals components. The characteristic length of the short-range structural forces, $\lambda_1$is one of the most sensitive parameters; a small variation in $\lambda_1$results in different forms of the disjoining/conjoining pressure isotherms (Fig.4, *a-c*) with various location of the primary and secondary minima. The parameter λ_2 changes the shape of the secondary minimum, but has a weaker influence on the shape of the isotherm.

An aqueous solution of a strong univalent electrolyte has been chosen with the bulk electrolyte concentration $c_0 = 1$ mole/m^3 and temperature $T = 293$ K for calculation in Fig.4. The electrostatic component of the disjoining/conjoining pressure was calculated for the case of constant surface charge density $\sigma_{s,h}$= const, with values σ_s= -150 mC and σ_h= 150 mC at the boundaries. The arbitrary values of the van der Waals and structural interaction parameters are used.

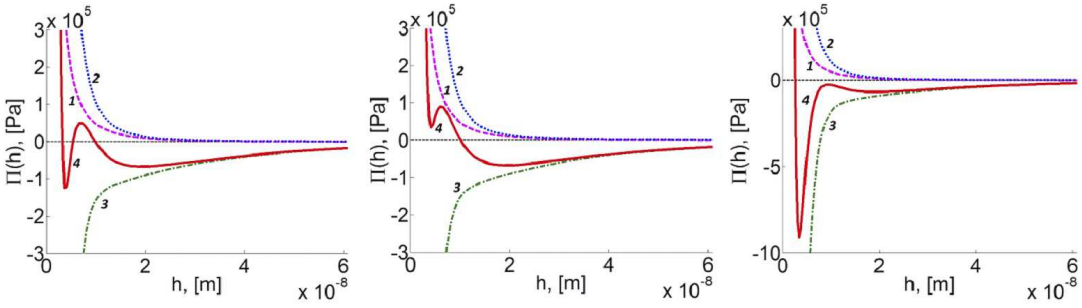

(a) (b) (c)

FIGURE 4. The disjoining/conjoining pressure isotherms according to Eq (2.4). The components of disjoining/conjoining pressure: 1- electrostatic, Π_E; 2 - van der Waals, Π_W; 3 - structural, Π_S; 4 - total interaction, $\Pi = \Pi_E + \Pi_W + \Pi_S$. Parameters of the electrostatic interaction: constant surface charge, σ_s= -150 mC; σ_h= -150 mC; $c_0 = 1$ mole/m^3, $T = 293$ K. Parameters of the van der Waals and structural interactions: $A = 2\times10^{-18}$ J; K_1 = -3.7×10^7 Pa; K_2 = -2×10^5 Pa; $\lambda_2 = 25\times10^{-9}$ m. *a)* $\lambda_1 = 1.35\times10^{-9}$ m; *b)* 1.31×10^{-9}; *c)* 1.5×10^{-9}.

In the case of the short-range structural repulsion, the parameter K_1 in Eq.(2.2) is positive and the structural components dependences take the shape presented in Fig.5*a*. In this situation the structural forces change a sign: they are repulsive or attractive depending on the distance. Now the disjoining/conjoining pressure isotherm can also include two minima (Fig.5*b*), but the both minima are possible if the short-range structural repulsion is counterbalanced by attractive electrostatic or van der Waals components. In Fig.5*b* the electrostatic force (curve 1) acts oppositely to the structural and van der Waals components (curves 3 and 2, respectively). The attractive (negative) values of the electrostatic component in Fig.5*b* were obtained for the different signs of the charged surfaces (σ_s= -150 mC; σ_h= 150 mC). The isotherms with different location of the primary minimum (similar to the isotherms shown in Fig.4*b* and *c*) can be obtained from data of Fig.5*b* by the variation of λ_1 parameter.

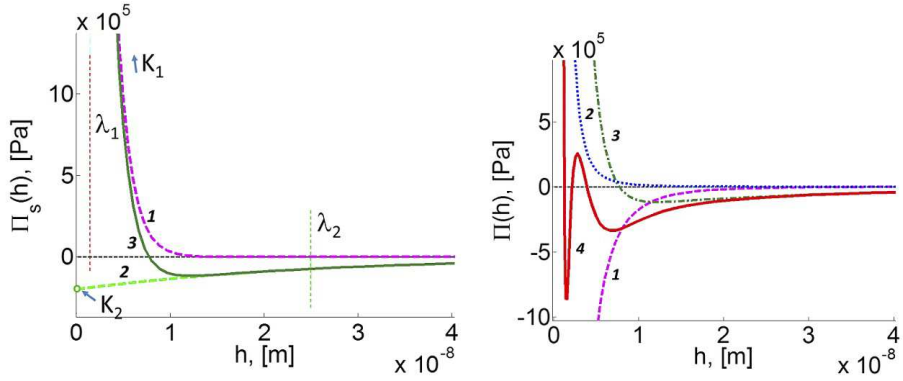

(a) (b)

FIGURE 5. The components of the structural interaction (*a*) and the disjoining/conjoining pressure isotherm (*b*) for the case of short-range structural repulsion ($K_1 > 0$). $K_1 = 3\times10^7$ Pa; $\lambda_1 = 1.45\times10^{-9}$ m; K_2 = -2×10^5 Pa; $\lambda_2 = 25\times10^{-9}$ m. *a*: 1,2,3 – the short-range, long-range and total structural interaction, respectively. *b*: 1,2,3,4 – the electrostatic, van der Waals, structural and total interaction, respectively.

Thus, the disjoining/conjoining pressure isotherms with two minima are possible if they include the structural interaction consisting of two parts acting at different distances: the long-range interaction is always attractive; the short-range one can be attractive or repulsive. As will be shown later, these features of the disjoining/conjoining pressure isotherms cause the characteristics of the contact angle hysteresis.

3. Hysteresis of contact angle in capillaries

In this section we briefly consider equilibrium of a meniscus in a flat capillary according to [1,2, 6].

If a meniscus is at equilibrium with a reservoir under the equilibrium pressure P_e, then there is no flow in the system. However, if the pressure inside the reservoir is changed by $\Delta P \neq 0$, then the flow will start immediately. In this case it is possible to divide the whole system (Fig. 6) into several regions: region 1, which is the spherical meniscus with a new radius, r, in a state of a new local equilibrium, a part of the transition region 2 in a state of a local equilibrium with a meniscus 1. Inside the regions 1 and 2 the pressure is constant everywhere and equals the new excess pressure, $P = P_e + \Delta P$; region *3* of a thin flat equilibrium thin film, where the pressure equals the initial equilibrium excess pressure, P_e; transport region *2'* in which a viscous flow of liquid occurs and in which the pressure gradually changes from the value P to P_e (Fig. 6). The largest pressure drop and the higher resistance to the flow occur in the non-equilibrium part of the transition region, 2', where the liquid film is very thin. Region *2'* covers a part of the transition region of very thin films, which immediately adjoins the equilibrium thin film.

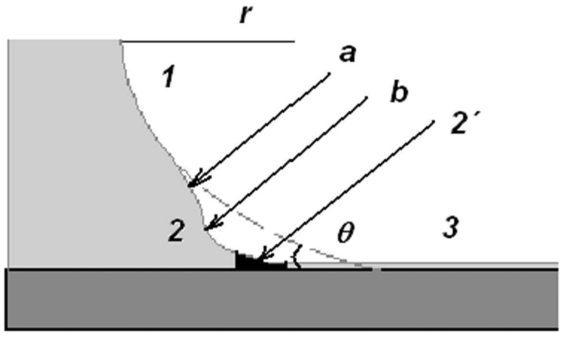

FIGURE 6. The liquid profile in a capillary in the case of partial wetting in the state of local equilibrium at excess pressure $P \neq P_e$; r and θ are the radius of the spherical meniscus in the central part of the capillary and the new local equilibrium contact angle, $\theta \neq \theta_e$. 1 – spherical meniscus of a new radius r, where $r \neq r_e$; 2 – profile of a part of the transition zone at local equilibrium with the meniscus; 3 – flat equilibrium liquid film of thickness h_e, with old equilibrium excess pressure P_e; 2'- a flow zone inside the transition region.

Keep in mind that the capillary is in contact with the reservoir, where the pressure, P_a- P_e-ΔP, is maintained, i.e., the pressure in the reservoir is lower than the atmospheric pressure, P_a.

If we increase the pressure under the meniscus then the meniscus does not move but changes its curvature to compensate for the excess pressure and, as a consequence, the contact angle increases accordingly. In this state the meniscus does not move macroscopically but it moves microscopically. This state of microscopic motion can continue infinitely if we neglect evaporation/condensation processes. The meniscus does not move macroscopically until some critical pressure and critical contact angle, θ_a, are reached. After further increase in pressure the flow zone occupies the region of much thicker β-films [1,2] and the meniscus starts to advance macroscopically. A similar phenomenon takes place if we decrease the pressure under the meniscus: it does not recede until a critical pressure and corresponding critical

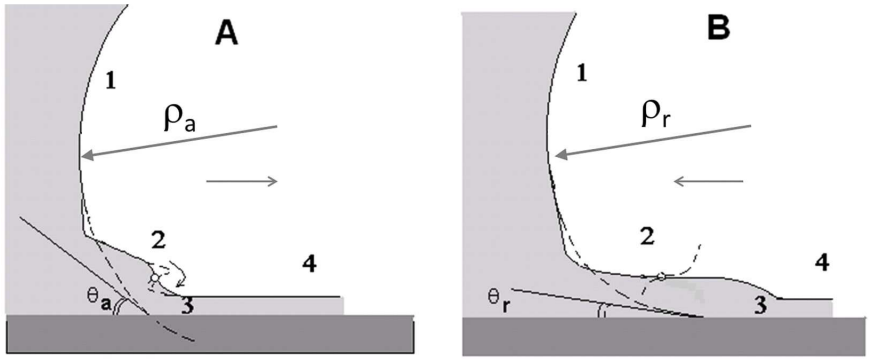

FIGURE 7. Contact angle hysteresis in capillaries in the case of partial wetting (s-shaped isotherm of Derjaguin's pressure). A - advancing contact angle: 1- a spherical meniscus of radius ρ_a; 2 - transition zone with a "dangerous" marked point (see explanation in the text); 3 - flow zone; 4 - flat film. Close to the marked point a dashed line shows the profile of the transition zone just after the contact angle reaches the critical value θ_a, the beginning of a "caterpillar motion". B - receding contact angle: 1- a spherical meniscus of radius $\rho_r < \rho_a$; 2 - transition zone with a "dangerous" marked point (see explanation in the text); 3 - flow zone, 4 - flat film. Close to the marked point the dashed line shows the profile of the transition zone just after the contact angle reaches the critical value θ_a.

contact angle, θ_r, are reached. This means that in the whole range of contact angles, $\theta_r < \theta < \theta_a$, the meniscus does not move macroscopically.

The above qualitative explanation for the contact angle hysteresis on smooth, homogeneous solid substrates is based on the s-shaped isotherm of disjoining/conjoining pressure in the case of partial wetting. The s-shaped determines a very special shape of the transition zone in the case of equilibrium meniscus (Fig. 6). In the case of increasing the pressure behind the meniscus (Fig. 7A) a detailed consideration [1,2] of the transition zone shows that close to the "dangerous" point marked in Fig. 7A, the slope of the profile becomes steeper with increasing pressure. In the range of very thin films (region 3 in Fig. 7A) there is a flow zone. Viscous resistance in this region is very high, that is why the meniscus advances very slowly. After some critical pressure behind the meniscus is reached, then the slope at the "dangerous" point reaches $\pi/2$. After that the flow step-wisely occupies the region of thick β-films the fast "caterpillar motion" starts as shown in Fig.7A.

In the case of decreasing the pressure behind the meniscus the event proceeds according to Fig. 7B. In this case up to some critical pressure the slope in the transition zone close to the "dangerous" marked point becomes more and more flat. In the range of very thin film (region 3 in Fig. 7B) there is a zone of flow. Viscous resistance in this region again is very high, that is why the receding of the meniscus proceeds very slowly. After some critical pressure behind the meniscus is reached then the profile in the vicinity of the "dangerous" point shows the discontinuous behaviour, which is obviously impossible. This means the meniscus will start to slide along the thick β-film. This phenomenon (the presence of a thick β-film behind the receding meniscus of aqueous solutions in quartz capillaries) has been discovered experimentally [17-18]. This supports our arguments explaining *static* contact angle hysteresis on smooth, homogeneous substrates.

The suggested mechanism of contact angle hysteresis on smooth homogeneous surfaces has a direct experimental confirmation [30,31].

The expressions for advancing and receding contact angles via Derjaguin's pressure isotherm were deduced in [1,2].

4. Equilibrium contact angle and disjoining/conjoining pressure for sessile droplets

According to [1,2] the equilibrium profile of a sessile two dimensional droplet is described by the following equation:

$$\frac{\gamma h''}{(1+h'^2)^{3/2}} + \Pi(h) = P_e, \tag{4.1}$$

where γ is the liquid-vapour interfacial tension, *h(x)* is an equilibrium droplet profile. According to the Kelvin's law

$$P_e = \frac{RT}{v_m} \ln \frac{p_s}{p} = -\frac{\gamma}{\rho}, \tag{4.2}$$

where v_m the molar liquid volume, p_s and p are saturated vapour pressure and the pressure of the vapour, which the sessile droplet is at equilibrium with. See Fig.8 for details. According to Eq (4.2) the liquid can be at equilibrium with oversaturated vapour only, that is if $p>p_s$. It is very difficult to keep oversaturated vapour over sessile droplet over a prolong period of time. This explain why equilibrium sessile droplets is so difficult (if possible at all) to investigate experimentally.

According to Eq. (4.1) the whole profile of a drop can be subdivided into three parts (Fig. 8): a spherical cap (using this part a *macroscopic* contact angle can be determined), a transition zone, where both capillary pressure and disjoining/conjoining pressure are equally important, and a flat equilibrium liquid film region ahead of the drop.

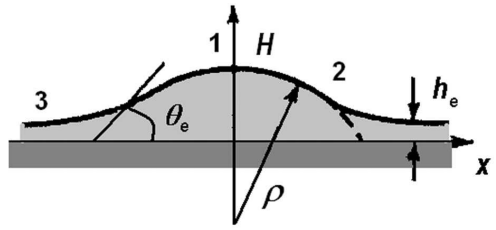

FIGURE 8. Equilibrium drop. 1 – spherical cap, where capillary forces dominate, 2 – transition zone, where capillary forces and disjoining/conjoining pressure are equally important, and 3 – flat equilibrium film in front of the drop.

The second order differential equation (4.1) can be integrated once, that gives:

$$\frac{1}{\sqrt{1+h'^2}} = \frac{C - P_e h - \int_h^\infty \Pi(h)dh}{\gamma}, \tag{4.3}$$

where C is an integration constant to be determined.

As due to the transversality condition $h'(h_e) = 0$ [19], the integration constant in Eq. (4.3) is $C = \gamma + P_e h_e + \int_{h_e}^\infty \Pi(h)dh$. Hence, the drop profile is described by the following equation:

$$\frac{1}{\sqrt{1+h'^2}} = \frac{\gamma - \phi(h, P_e)}{\gamma} \tag{4.4}$$

where

$$\phi(h, P_e) = -P_e\,(h - h_e) + \int_{h_e}^{h} \Pi dh. \tag{4.5}$$

As the left hand side of Eq. (4.4) is always positive and also less or equal to unity, it demands that:

$$0 \le \phi(h, P_e) \le \gamma, \tag{4.6}$$

where the first condition corresponds to a zero derivative h', and the second one corresponds to an infinite value of h'.

On the other hand at the drop apex, H, the derivative vanishes, $h'(H) = 0$. This together with Eq. (4.3) results in $C = \gamma + P_e H$. Then Eq. (4.3) becomes

$$\frac{1}{\sqrt{1+h'^2}} = \frac{\gamma + P_e(H-h) - \int_h^\infty \Pi(h)dh}{\gamma}. \tag{4.7}$$

Outside the range of the disjoining/conjoining pressure action Eq. (4.7) reduces to

$$\frac{1}{\sqrt{1+\bar{h}'^2}} = \frac{\gamma + P_e(H-\bar{h})}{\gamma}, \tag{4.8}$$

which describes the spherical cap of the drop in Fig. 8. The magnitudes $\bar{h}'$ and $\bar{h}$ correspond to the spherical cap in the absence of surface forces. Intersection of the latter profile with the thin equilibrium film of thickness h_e defines an apparent three-phase contact line and the macroscopic equilibrium contact angle: $\bar{h}'(\bar{h}=0) = -\tan\theta_e$. Then Eq. (4.8) can be rewritten at $\bar{h}=0$ as $P_e = -\frac{\gamma(1-\cos\theta_e)}{H}$. Casting this expression into Eq. (4.7) at $h{=}h_e$ results in the following expression of the contact angle in the case of drops on a flat substrate:

$$\cos\,\theta_e = 1 + \frac{\frac{1}{\gamma}\int_{h_e}^{H}\Pi(h)dh}{1-h_e/H} \approx 1 + \frac{1}{\gamma}\int_{h_e}^{\infty}\Pi(h)dh, \quad \text{for} \quad t_s << H. \tag{4.9}$$

where $t_s \approx 100$ nm is the radius of surface forces action. Eq.(4.9) is also known as Frumkin-Derjaguin equation [28,29]. As follows from (4.9), for the *partial* wetting case

$$\int_{h_e}^{\infty}\Pi(h)dh < 0. \tag{4.10}$$

Note that the equilibrium contact angle defined by Eq. (4.9) is not completely determined by the shape of the disjoining/conjoining pressure isotherm: it also depends on the lower limit of integration, h_e, which is determined by the equilibrium excess pressure P_e. In other words, the *equilibrium* contact angle of drops depends on the *equilibrium* volume of the drop, which can vary from "infinity" (at $P_e{=}0$) to a minimum value at $P_e{=}\Pi_{min}$ (Fig. 9).

Fig. 9 illustrates the dependence of the disjoining/conjoining pressure on the thickness of a flat liquid film for the cases of *complete* wetting (curve 1, which corresponds to $\Pi_M(h)$ typical for oil drops on glass substrates) and *partial* wetting (curve 2, which corresponds to Eq. (4.10), typical for aqueous electrolyte solutions on glass substrates).

5. Static hysteresis of contact angle of sessile droplets on smooth homogeneous substrates

The derivation of Eq. (4.1) shows that it determines a single, unique equilibrium contact angle (at fixed external conditions). Experiments, however, show contact angle hysteresis with an infinite number of apparent "quasi-equilibrium positions" and "quasi-equilibrium contact angles" of a drop on a solid surface such that $\theta_r{<}\theta{<}\theta_a$, where θ_r and θ_a are denoted as (static) *receding* and *advancing* contact angles. Indeed, let us consider a liquid drop on a horizontal substrate, which is slowly growing by pumping through an orifice in the substrate (Fig.10). After we stop pumping liquid just before the droplet starts advancing a static advancing contact angle, θ_a, is formed. Any further pumping will result in subsequent drop spreading. Let us now consider the reverse experiment. If we start from the static advancing contact angle, θ_a, reached as described above and if we start sucking the liquid through the same orifice, then

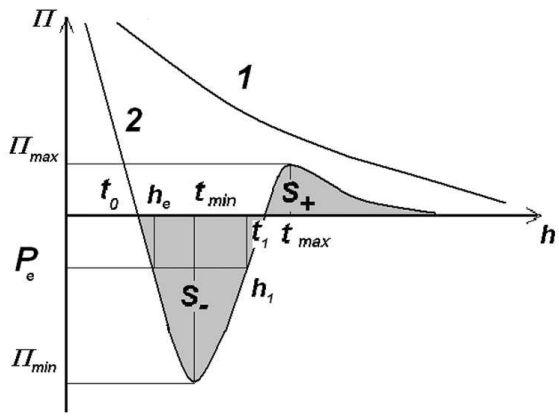

FIGURE 9. Disjoining/conjoining pressure isotherms: 1 – complete wetting, 2 – partial wetting. The value h_e defines the equilibrium thickness of equilibrium flat films in the case of drops. Note, there are two solutions of the equation $\Pi(h_e) = P_e$. However, only one of them satisfies the thermodynamic stability condition $d\Pi(h_e)/dh < 0$ [1,2].

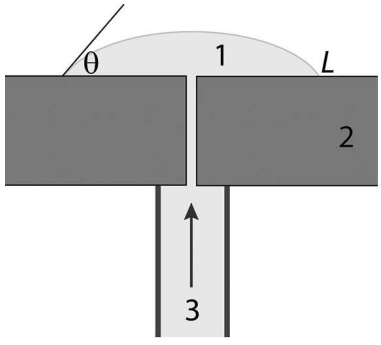

FIGURE 10. Schematic illustration of the formation of a drop by appropriate liquid pumping. L-radius of the drop base; θ - contact angle. 1- liquid drop, 2- solid substrate with a small orifice in the center, 3 - liquid source/sink (syringe).

the contact angle will decrease without the drop base shrinking until another critical contact angle, θ_r, is reached; after further pumping the liquid out the drop recedes and eventually disappears. For water drops on smooth homogeneous glass surfaces, $\theta_r \approx 0\text{-}5^o$, while θ_a is in the range of $40\text{-}60^o$.

It is possible to show [1,2] that the height of equilibrium sessile drops, H, decreases with increasing *over*saturation, when the value of P_e decreasing. However, this decrease has certain limits, since drops can be at the equilibrium with flat films only if $P_e > \Pi_{min}$ (Fig. 9). It can be seen from Fig. 9, curve 2, that Π_{min} is the pressure corresponding to the minimum of the isotherm $\Pi(h)$. For $P_e < \Pi_{min}$ there is neither a film nor a drop on the surface at equilibrium. When P_e decreases and approaches Π_{min}, drops whose size diminishes, should be "torn" off the surface and pass into the vapor phase.

Maintaining the external conditions, we consider now non-equilibrium profiles of drops when their volumes change by pumping liquid in or out (see Fig. 10) and the excess pressure P is different from the equilibrium value. As in [1,2] we assume that the main part of the liquid profile is still described by Eq. (4.1), where the equilibrium pressure, P_e, is replaced now by a new non-equilibrium pressure, P:

$$\frac{\gamma h''}{(1+h'^2)^{3/2}} + \Pi(h) = P. \tag{5.1}$$

Qualitative reason for that assumption is presented in Fig. 6 for the case of a meniscus.

5.1. Expressions for the advancing contact angle

Advancing contact angles are formed if $P < P_e$. The condition for the existence of a solution for Eq. (5.1) is written for a drop in the following form:

$$\gamma \geq \varphi\,(h, P) \geq 0, \tag{5.2}$$

where now the function $\varphi(h,\ P)$ is given by:

$$\varphi\,(h, P) = -P\,(H - h) + \int_h^\infty \Pi\,(h)\,dh. \tag{5.3}$$

Examples of the form of the function $\varphi(h,\ P)$ (curves *2-3)* for the disjoining/conjoining pressure isotherm $\Pi(h)$ are shown in Fig. 11. The extrema of $\varphi(h,\ P)$ are found from the condition $P = \Pi(h)$, just as in the case of equilibrium, i.e., from the points of intersection of the disjoining/conjoining pressure isotherm with the straight line $P = const$. It follows from Eq. (5.3) that for equilibrium profile of a drop, i.e., for $P = P_e$, the function $\varphi(h,\ P_e)$ vanishes at $h = h_e$. On the other hand $\varphi(h,\ P_e)$ vanishes also at $h = H$. Since $\varphi(h,\ P_e) > 0$, the function $\varphi(h,\ P_e)$ has a maximum for $h = h_2$ (Fig. 11, curve 2).

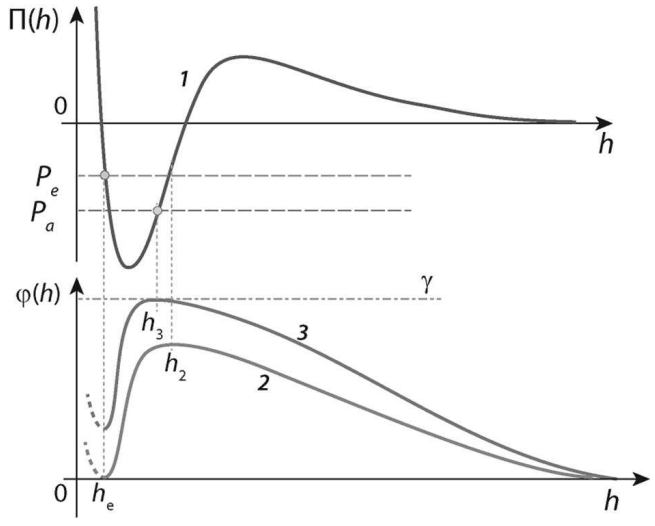

FIGURE 11. Disjoining/conjoining pressure isotherm $\Pi(h)$. The upper figure: the case of *partial* wetting (curve 1); and lower figure: corresponding curves (2, 3) of the functions φ (5.3) determining the conditions of equilibrium (curve 2) or quasi-equilibrium of a drop before the advancing starts (curve 3).

At lower pressures, for $P < P_e$, the drop surface becomes more convex than at equilibrium, the line $\varphi(h,\ P)$ (Figure 11, curve 3) is located above the equilibrium curve 2. The condition of quasi-equilibrium is violated and the perimeter of the drop starts to advance after the maximum of $\varphi(h,\ P)$ reaches the dashed line $\gamma = const$ (curve 3). This condition corresponds to the appearance of a thickness with a vertical tangent $h' = \infty$ on the profile of the drop. Then liquid flows from the drop to the film by the so-called Frenkel's "caterpillar" mechanism if $\varphi(h,\ P) > \gamma$. This shows that the static *advancing* contact angle does not depend on the roughness of a solid substrate if the roughness size is below the value of $h_3 \sim$10-30 nm, a phenomenon well known experimentally.

Let us calculate the value of the *advancing* contact angle θ_a, using the condition $\varphi(h,\ P)=\gamma$:

$$-P_a\left(H_a-h_3\right)+\int_{h_3}^{\infty}\Pi\left(h\right)dh=\gamma. \tag{5.4}$$

Keeping in mind that $P_a = \gamma\ (cos\ \theta_a\text{-}1)/H_a$, it follows that

$$\cos\theta_a=\frac{P_a h_3}{\gamma}+\frac{1}{\gamma}\int_{h_3}^{\infty}\Pi(h)dh\approx\frac{1}{\gamma}\int_{h_3}^{\infty}\Pi(h)dh. \tag{5.5}$$

Let us calculate the difference $\cos\theta_e-\cos\theta_a$ using Eq. (4.9) for the equilibrium contact angle, θ_e, equilibrium excess pressure, P_e, in the drop, and Eq. (5.5). We obtain

$$\cos\theta_e-\cos\theta_a=1+\frac{1}{\gamma}\int_{h_e}^{h_3}\Pi(h)dh>0, \tag{5.6}$$

The latter shows that $cos\ \theta_e > cos\ \theta_a$ and $\theta_a > \theta_e$. Thus, in the case of a drop, the suggested theory shows in agreement with experimental observations that the *advancing* angle is always bigger than the *equilibrium* angle.

If we assume that the disjoining/conjoining pressure isotherm changes very abruptly between t_{min} and t_1 (Fig. 9), then $h_3\approx t_{\min}\approx t_1 = const$. The latter assumption is partially supported by the curve 1 in Fig. 9. In this case Eq. (5.5) gives

$$\cos\theta_a=\frac{S_+}{\gamma}. \tag{5.7}$$

In general the *advancing* contact angle can be determined in the following way. From equation $P_a=\Pi(h_3)$ we get P_a as a function of the thickness h_3. Since the latter equation has two solutions, the second root (not the first) should be selected (Fig. 11, curve 3). Using this solution in Eq. (5.4) yields $-\Pi(h_3)\left(H_a-h_3\right)+\int_{h_3}^{\infty}\Pi\left(h\right)dh=\gamma$, that provides the unknown height of the drop H_a as a function of h_3:

$$H_a=h_3+\frac{\gamma-\int_{h_3}^{\infty}\Pi\left(h\right)dh}{-\Pi(h_3)}, \tag{5.8}$$

where $P_a=\Pi(h_3)<0$ and $\gamma-\int_{h_3}^{\infty}\Pi\left(h\right)dh>0$.

Let R_a be the radius of curvature of the drop at the moment of advancing. A simple geometrical consideration shows that

$$L_a=R_a\sin\theta_a=-\frac{\gamma\sin\theta_a}{\Pi(h_3)}, \tag{5.9}$$

where L_a is the radius of the droplet base at the moment when advancing contact angle is reached. The volume of the drop at the moment of advancing, V_a, can be expressed as

$$V_a=\frac{L_a^2}{\sin^2\theta_a}\left(\theta_a-\sin\theta_a\cos\theta_a\right). \tag{5.10}$$

Note that according to experimental condition, the volume V_a is fixed but not the radius of the droplet base, L_a. From Eq. (5.10) we conclude:

$$L_a=\sin\theta_a\sqrt{\frac{V_a}{\left(\theta_a-\sin\theta_a\cos\theta_a\right)}}. \tag{5.11}$$

Combination of Eqs. (5.9) and (5.11) results in

$$\sqrt{\frac{V_a}{\left(\theta_a-\sin\theta_a\cos\theta_a\right)}}=-\frac{\gamma}{\Pi(h_3)}, \tag{5.12}$$

where the contact angle θ_a is expressed as

$$\cos\theta_a = \frac{\Pi(h_3)h_3}{\gamma} + \frac{1}{\gamma}\int_{h_3}^{\infty} \Pi(h)dh. \tag{5.13}$$

and sin $\theta_a = \sqrt{1-\cos^2\theta_a}$.

The values h_3 and θ_a are found as a solution of Eqs.(5.12)-(5.13).

Thus, our theory predicts a dependency of the advancing contact angle on the droplet volume V_a. It is clearly shown now that static *advancing* contact angle in the case of drops is not a unique characteristic of solid substrates but determined also by the external conditions.

The latter conclusion was confirmed experimentally in [20-23]. In [21,22] the authors showed that the advancing contact angle of droplets really increases as the volume of the droplet decreases. In [20,23] the advancing contact angle of bubbles was considered and the authors arrived to the same conclusion. It should be noted that the experimental results on the contact angle hysteresis on smooth homogeneous surfaces are very rare in the literature. The theoretical models of this phenomenon are frequently based on various concepts [24, 25], where action of surface forces is not taken into account.

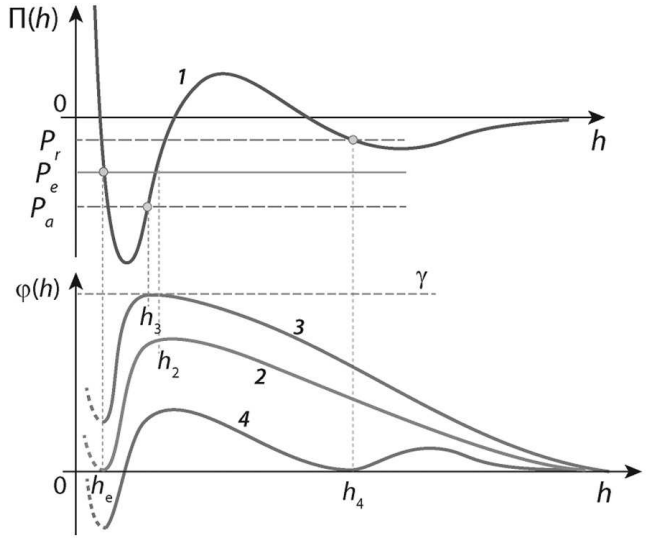

FIGURE 12. Disjoining/conjoining pressure isotherm $\Pi(h)$. The upper figure: the case of *partial* wetting (curve 1); and lower figure: corresponding curves (2, 3, 4) of the functions φ (5.3) determining the conditions of equilibrium (curve 2) or quasi-equilibrium of a drop before the advancing starts (curve 3) and before the receding starts (curve 4).

At higher pressures, i.e., for $P > P_e$, when the drop surface becomes less convex, the line $\varphi(h, P)$ (Figure 12, curve 4) is located below that of the equilibrium curve 2. The condition of quasi-equilibrium is violated and the perimeter of the drop starts to recede after the minimum of $\varphi(h, P)$ reaches zero (curve 4). This condition corresponds to the appearance of a thickness with a horizontal tangent $h' = 0$ on the profile of the drop. After that the droplet starts sliding over thick β – film.

5.2. Expressions for the receding contact angle

The expressions for the receding contact angle are found using the condition $\varphi(h, P)=0$:

$$P_r\,(H_r - h_4) + \int_{h_4}^{\infty} \Pi dh = 0 \tag{5.14}$$

From Eq.(5.14) the droplet height at the moment of receding is

$$H_r = h_4 + \frac{1}{P_r}\int_{h_4}^{\infty} \Pi dh \tag{5.15}$$

For the spherical droplet:

$$P_r = \gamma(\cos\theta_r - 1)\ /H_r \tag{5.16}$$

The receding contact angle is expressed from Eqs.(5.16) and (5.14) as

$$\cos\theta_r\ = 1 + \frac{P_r H_r}{\gamma} = 1 + \frac{P_r h_4}{\gamma} + \frac{1}{\gamma}\int_{h_4}^{\infty} \Pi dh \tag{5.17}$$

It is assumed that the droplet base does not shrink during the transition between the advancing and receding angles, i.e. L_a=L_r= const.
Then the radius of the base contact line $L_r = R_r \sin\theta_r$ is expressed using Eq.(5.17) as

$$L_r = -\frac{\gamma}{\Pi\,(h_4)}\sqrt{1 - \left(1 + \frac{\Pi\,(h_4)\,h_4}{\gamma} + \frac{1}{\gamma}\int_{h_4}^{\infty} \Pi dh\right)^2} = L_a \tag{5.18}$$

The value h_4 is found from Eq.(5.18), where L_a is already known from Eq. (5.11). The receding volume is expressed as

$$V_r = \frac{L_a^2}{\sin^2\theta_r}\,(\theta_r - \sin\theta_r\cos\theta_r) \tag{5.19}$$

6. Conclusions

Based on the developed theory for contact angle hysteresis on smooth, homogeneous solid substrates in terms of the disjoining/conjoining pressure, it was shown that for any value of the contact angle, θ, from the range θ_r<θ<θ_a, except the equilibrium value $\theta = \theta_e$, a slow "microscopic" advancing or receding motion of the liquid takes place.

The expressions for the advancing and receding contact angles were obtained theoretically from analysis of the shape of the disjoining/conjoining pressure isotherm. At the moment of achievement of θ_r and θ_a, the "microscopic" motion is replaced by fast "macroscopic" motion leading to an abrupt transformation or destruction of the droplet.

It is shown that both advancing and receding contact angles of droplets on smooth homogeneous solid substrates depend on the droplet volume. This conclusion has a direct experimental confirmation.

The evaporation, which takes place more intensively in vicinity of the three-phase contact line [27], makes the measurements of both advancing and receding contact angles of drops not so straightforward and unambiguous in the case of volatile liquids. It is the reason why a number of experiments on wetting/spreading of liquids have been performed in thin capillaries, where evaporation can be significantly diminished if not ruled out.

Acknowledgements. This work was supported by CoWet ITN, EU, Engineering and Physical Sciences Research Council, UK, grant EP/D077869/1, ESA under grant PASTA, and COST MP1106 project; UK-Russia joint project, the Royal Society, UK.

References

[1] V M Starov, M G Velarde. *Surface forces and wetting phenomena.* J. Phys.: Condens. Matter, 21 (2009), 464121.
[2] V Starov, M Velarde, C Radke. Wetting and Spreading Dynamics. In "Surfactanrt Science Series", v. 138, Taylor&Francis, 2007, 515 pp.

[3] N. V. Churaev, V. D. Sobolev, V. M. Starov. *Disjoining Pressure of Thin Nonfreezing Interlayers.* J Colloid Interface Sci, 247 (2002), 80–83.

[4] N.V. Churaev, V.D. Sobolev. *Wetting of low energy surfaces.* Adv. Colloid Interf. Sci., 134–135 (2007), 15–23.

[5] I.V. Kuchin, O.K. Matar, R.V. Craster, V.M. Starov. *Influence of the disjoining pressure on the equilibrium interfacial profile in transition zone between a thin film and a capillary meniscus.* Colloid and Interface Science Communications, 1 (2014), 18-22.

[6] V. Starov. *Static contact angle hysteresis on smooth, homogeneous solid substrates.* Colloid Polym Sci, 291 (2013), 261–270.

[7] E. Chibowski. *Surface free energy of a solid from contact angle hysteresis.* Adv. Colloid Interface Sci., 103 (2003), 149–172.

[8] C. W. Extrand, Y. Kumagai. *An experimental study of contact angle hysteresis.* J. Colloid Interface Sci., 191 (1997), 378–383.

[9] C. W. Extrand. *Water contact angle and hysteresis of polyamid surfaces.* J. Colloid Interface Sci., 248 (2002), 136–142.

[10] Z.M. Zorin, V.D. Sobolev, N.V. Churaev. Surface Forces in Thin Films and Disperse Systems, Nauka, Moscow, 1972, p. 214. [in Russian].

[11] E.A. Romanov, D.T. Kokorev, N.V. Churaev. *Effect of wetting hysteresis on state of gas trapped by liquid in a capillary.* Int. J. Heat Mass Transfer, 16 (1973), 549-554.

[12] N.Rangelova, D.Platikanov, *Annals Univ. Sofia, Fac.Chim.,* 71/72, 109 (1976/1977); D. Platikanov, G.P. Yampolskaya, N. Rangelova, Zh. Angarska, L.E. Bobrova, V.N. Izmailova. *Free black films of proteins. Thermodynamic parameters.* Colloid J., USSR, 43 (1981), 177-180.

[13] N. Rangelova, D. Platikanov, *Annals Univ. Sofia, Fac. Chim.,* 78 (1984) 126.

[14] N.I. Rangelova, V.N. Izmailova, D.N. Platikanov, G.P. Yampol'skaya, S.D. Tulovskaya. *Free black films of proteins: dynamic hysteresis of the contact angle (film-bulk liquid) and the rheological properties of adsorption layers.* Colloid J., USSR, 52 (1990), 442-447.

[15] D. Platikanov, M. Nedyalkov, V. Petkova. *Phospholipid black foam films: dynamic contact angles and gas permeability of DMPC bilayer films.* Adv. Colloid Interface Sci., 101-102 (2003), 185-203.

[16] V. Petkova, D. Platikanov, M. Nedyalkov. *Phospholipid black foam films: dynamic contact angles and gas permeability of DMPC+DMPG black films.* Adv. Colloid Interface Sci., 104 (2003), 37-51.

[17] B.V. Derjaguin, Z.M. Zorin. *Investigation of the surface condensation and vapour adsorption close to saturation conditions with micropolarization method.* Zh. Fiz. Khim, 29 (1955) 1755-1770.

[18] Z.M. Zorin, A.V. Novikova, A.K. Petrov, N V. Churaev. Surface Forces in Thin Films and Stability of Colloids, Nauka, Moscow (1974), p.94 [in Russian].

[19] H. Sagan. Introduction to the Calculus of Variations, Dover reprint, New York, 1992, chapter 7.

[20] J. Drelich. *The Effect of Drop (Bubble) Size on Contact Angle at Solid Surfaces.* J. Adhesion, 63 (1997), 31-51.

[21] R.J. Good, M.N. Koo. *The Effect of Drop Size on Contact Angle.* J. Colloid Interface Sci., 71 (1979) 283-292.

[22] G.L. Mack. *The Determination of Contact Angles from Measurements of the Dimensions of Small Bubbles and Drops. I. The Spheroidal Segment Method for Acute Angles.* J Phys Chem., 40 1936, 159-167.

[23] V.S. Veselovsky, V.N. Pertsev. *Adhesion of the bubbles to solid surfaces.* J. Phys Chem (USSR Academy of Sciences), 8 (1936), 245-259 (in Russian).

[24] C.O. Timmons, W.A. Zisman. *The Effect of Liquid Structure on Contact Angle Hysteresis.* J. Colloid Interface Sci., 22 (1966) 165-171.

[25] A.M. Schwartz. *Contact Angle Hysteresis: A Molecular Interpretation.* J. Colloid Interface Sci., 75 (1980), 404-408.

[26] K.S. Lee, C.Y. Cheah, R.J. Copleston, V.M. Starov, K. Sefiane. *Spreading and evaporation of sessile droplets: Universal behavior in the case of complete wetting.* Colloids and Surfaces A: Physicochem. Eng. Aspects, 323 (2008) 63-72.

[27] S. Semenov, A. Trybala, R. Rubio, N. Kovalchuk, V. Starov, M. Velarde. *Simultaneous spreading and evaporation: Recent developments.* Adv Colloid Interface Sci, 206 (2014), 382–398.

[28] A.N. Frumkin. *About phenomena of wetting and adhesion of bubbles.* Zh. Fiz. Khim. 12 (1938), 337-345.

[29] B.V. Derjaguin. *Theory of capillary condensation and other capillary phenomena with taking into account the disjoining pressure of polymolecular liquid films.* Zh. Fiz. Khim. 14 (1940) 137-147.

[30] Z. M. Zorin, V. P. Romanov, N. V. Churaev.*The contact angles of surfactant solution on the quartz surface.* Colloid & Polymer Sci. 257 (1979), 968-972

[31] R.A. Hayes, J. Ralston. *Contact angle relaxation on low energy surfaces.* Colloids Surfaces, 80 (2-3) (1993), 137-146.